Thin Solid Films 519 (2011) 2302–2307

Contents lists available at ScienceDirect

Thin Solid Films

journal homepage: www.elsevier.com/locate/tsf

Estimation of compensation ratio by identifying the presence of different hopping conduction mechanisms in SnO_2 thin films

N. Serin [a], A. Yildiz [b,*], A.A. Alsaç [a], T. Serin [a]

[a] Department of Engineering Physics, Faculty of Engineering, Ankara University, 06100, Ankara, Turkey
[b] Department of Physics, Faculty of Science and Arts, Ahi Evran University, 40040, Kirsehir, Turkey

ARTICLE INFO

Article history:
Received 7 June 2010
Received in revised form 8 November 2010
Accepted 17 November 2010
Available online 2 December 2010

Keywords:
Conduction mechanism
Tin oxide
Nearest-neighbour hopping
Variable-range hopping
Compensation ratio

ABSTRACT

The electrical properties of undoped SnO_2 thin films prepared by the sol–gel technique were investigated by conductivity measurements in a temperature range of 50–200 K. Structural characterizations of the films were performed by atomic force microscopy and X-ray diffraction. Optical properties of the samples were also characterized by optical absorption spectroscopy. The different hopping models were used to investigate the characteristics of electrical conduction by hopping in employed temperature range. It was shown that three types of behavior can be expected, nearest-neighbour hopping at high temperatures, the Mott variable-range hopping at low temperatures and Efros–Shklovskii variable-range hopping at lower temperatures. The criteria for the observation of these three regions were established and the transitional behavior of the conductivity was determined. The experimentally determined critical transition temperatures were at the orders of magnitudes with what could be expected based on hopping conduction calculations. Under these analyses, the compensation ratio of the films was determined.

1. Introduction

SnO_2 exhibits considerably high defect concentrations despite a remarkable progress in its crystal quality over the past years [1]. In order to gain full control over the materials properties, therefore, the understanding of the physics of defects in the material is very important. The presence of disorder in the material drastically changes the electrical conduction mechanism. Then, a decrease in the conductivity is generally expected due to the existence of disorder. Recently, we have reported the effect of the presence of defects on conductivity of undoped and Sb-doped SnO_2 thin films [1]. In disordered systems, the Arrhenius type temperature dependence in the conductivity can be observed, if carriers are thermally activated across mobility edges into the extended states. However, it is possible to observe different conduction mechanisms depending on film structure and the measurement temperature region. Generally, the hopping conduction at low temperatures is considered to be the dominant transport mechanism in disordered systems [2–6].

One can expect different degrees of disorder to arise in SnO_2 depending on the preparation conditions. Conductivity measurements in undoped SnO_2 indicate the hopping conduction behavior at low temperatures [1]. The electrical properties of semiconductors are very sensitive to the degree of compensation of the material. Therefore, it is of great importance for one to determine the concentration of donors (N_D) and acceptors (N_A) concerning the electrical properties of SnO_2. However, up until now, the compensation ratio, k ($k = N_A/N_D$ for n-type material) of SnO_2 has not been determined by correctly identifying the presence of different hopping conduction mechanisms in the material.

In this report, we present the electrical conductivity behavior over the temperatures (50–200 K) for SnO_2 films prepared by sol–gel technique. The parameters of N_D, N_A and then k of SnO_2 were determined using the conductivity measurements data.

2. Experimental

The 1 mm thick rectangular shaped (26×76 mm^2) glass substrates were ultrasonically cleaned in de-ionized water and acetone (CH_3-$COCH_3$, Merck) for 30 min. They were dried in the furnace at 100 °C for 10 min. The SnO_2 solution was obtained by means of dissolving 8.37 g of stannous chloride $SnC1_22H_20$ in 100 ml of absolute ethanol [C_2H_6O, Merck]. The solution was stirred and heated in a closed vessel. Then the vessel was opened, and the solution again stirred and heated until the solvents were completely evaporated. Finally, powders were obtained. Then, powders were dissolved in 50 ml of absolute ethanol. The solution was finally stirred and heated at 50 °C for 2 h. The cleaned glass substrates were dipped into the solution and withdrawn at a constant speed of 80 mm min^{-1}. Each coating on glass substrate was heated at 500 °C for 10 min in the furnace. This process coating was repeated to get the desired film thickness. The thickness of the films was determined as 630 nm and 940 nm by means of optical transmission spectrum using the envelope method [7].

* Corresponding author. Tel.: +90 386 252 80 50; fax: +90 386 252 80 54.
E-mail address: yildizab@gmail.com (A. Yildiz).

0040-6090/$ – see front matter © 2010 Elsevier B.V. All rights reserved.
doi:10.1016/j.tsf.2010.11.027

The microstructure of the deposited films was investigated by means of an Inel-EQUINOX 1000 diffractometer. The radiation source, wavelength, and scanning range 2θ of the diffractometer were Co K_α, 0.179 nm, and 15° to 70°, respectively.

The optical absorption studies were carried out by using UV–Vis–NIR spectrophotometer Model UV 3600 in the spectral range 300–1500 nm. The electrical conductivity measurements were carried out using Keithley 2420 programmable constant current source in a temperature range of 50–200 K.

The surface morphology of the films was also observed by a Solver-PRO (NT-MDT) in semi-contact mode. The root mean square (RMS) values of surface roughness were estimated.

3. Results and discussion

The X-ray diffraction (XRD) patterns of SnO_2 films shown in Fig. 1 exhibited three sharp peaks and some weak peaks corresponding to (110), (101), (211) and (200), (220), (310), (301) planes, respectively. Thus, the films are polycrystalline in nature. A matching of the observed and the standard (h k l) planes confirm that the deposited films are of SnO_2 having primitive tetragonal structure [8]. The films showed the preferred orientations along (101) plane. The lattice constants a and c for the tetragonal phase structure are determined by the relation,

$$\frac{1}{d^2} = \left(\frac{h^2}{a^2} + \frac{k^2}{a^2}\right) + \left(\frac{l^2}{c^2}\right) \quad (1)$$

where d and (hkl) are the inter planer distance and Miller indices, respectively. The lattice constants a and c are calculated and given in Table 1. It was observed that lattice constants calculated match well with the standard JCPDS data card [8].

In order to determine the variation of the crystallite size, the size of the crystallites oriented along (101) plane is calculated using Scherrer's formula [9]

$$L = \frac{0.9\lambda}{B\ cos\theta} \quad (2)$$

where B, θ and λ are the broadening of diffraction line measured at half its maximum intensity in radians, the diffraction angle and the X-ray wavelength, respectively. The calculated values of crystallite size are given in Table 1. The crystallite size increases with the increase of thickness (Table 1).

The optical band gaps of the films have been determined on the basis of UV–Vis–NIR transmission measurements. For this, the fundamental absorption coefficient (α) was evaluated using $\alpha = (\ln T^{-1})/t$ where t is the film thickness and T is the transmittance. Since SnO_2 declared as direct band gap nature of the material in the literature [10], it was utilized from the relation [11]

$$\alpha h\nu = A\left(h\nu - E_g\right)^{1/2} \quad (3)$$

in order to determine the band gap of the SnO_2 film, where $h\nu$ is the photon energy, E_g is the optical band gap energy and A is a constant. The typical plot of $(\alpha h\nu)^2$ vs. $h\nu$ is depicted in Fig. 2. It is linear indicating the presence of direct transition. The linear portion is extrapolated to $\alpha = 0$, on energy axis, which gives the band gap energy of 3.76 eV and 3.74 eV for the 630-nm and 940-nm thickness, respectively. These values correspond to those given in the literature by different authors (values varying between 3.60 eV and 3.95 eV depending on the elaboration methods [12–14]).

The surface morphology of the films is shown in Fig. 3. Atomic force microscopy (AFM) analysis showed that films are polycrystalline and have needle-shaped nano grains. The RMS values of surface roughness were estimated and given in Table 1. The average crystallite size and root mean square roughness increase with the increase of the thin film thickness, while the surface area of the crystallite boundaries decreases.

Fig. 4 shows the variations of electrical conductivity (σ) with temperature for the samples. By comparing these two curves, it is noted that there is a significant increase in the conductivity of SnO_2 after decreasing thickness of film. Also, as mentioned previously, the value of the conductivity decreases with increasing crystallite size (Table 1). Since a polycrystalline film has crystallites joined at their surfaces via grain boundaries, the boundaries between crystallites play an important role in determining the conductivity of polycrystalline film. According to grain boundary model [15,16], an increase in the crystallite size causes a decrease in grain boundary scattering and this leads to an increase in the conductivity. Generally, grain boundary model can be also applicable at high temperatures [15,16]. However, the conductivity behavior in our case may not be inferred by grain boundary model [15,16], since the conductivity does not increase as crystallite size increases in our case. We should also mention here that the electrical conductivity does not increase decreasing activation energy (barrier potential energy) in the investigated films. Here,

Table 1
Structural parameters of the investigated SnO_2 films.

Sample	a (nm)	c (nm)	c/a	L (nm)	RMS (nm)
Thickness (630 nm)	0.472 ± 0.05	0.311 ± 0.05	0.66	5.40	0.720
Thickness (940 nm)	0.480 ± 0.05	0.317 ± 0.05	0.66	6.97	1.012

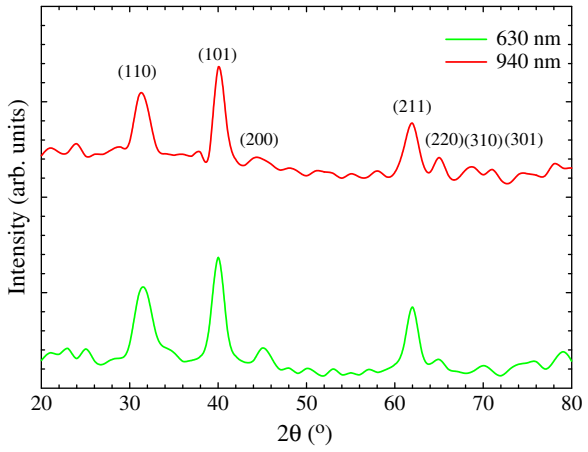

Fig. 1. XRD patterns of SnO_2 films.

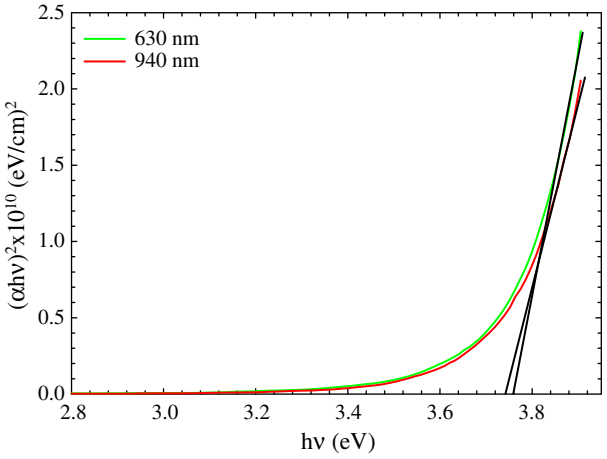

Fig. 2. Plot of $(\alpha h\nu)^2$ vs. $h\nu$ for SnO_2 films.

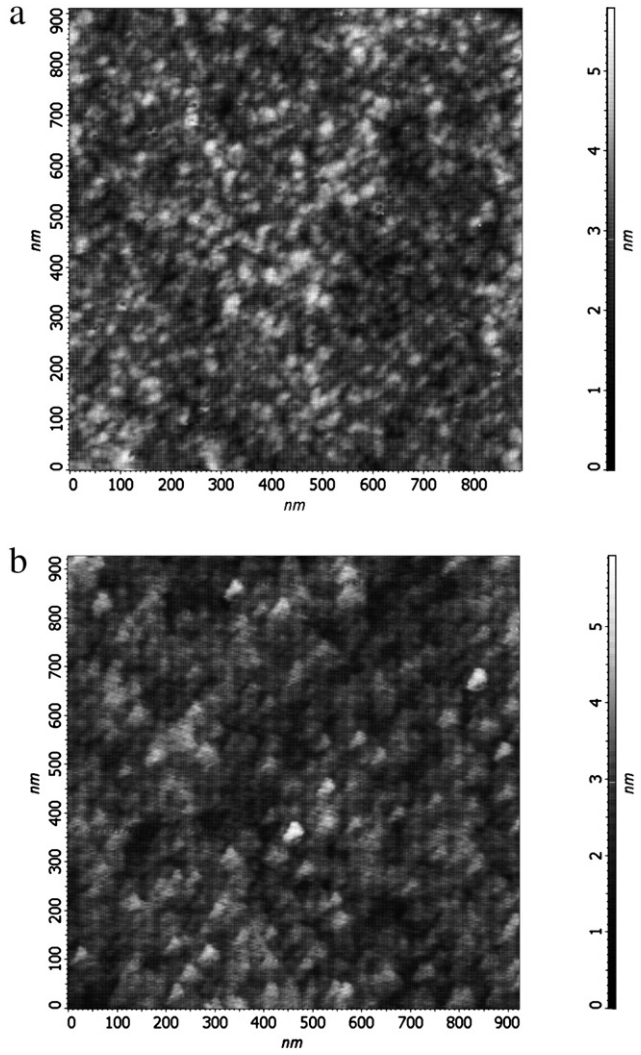

Fig. 3. Two-dimensional (2D) AFM images for samples a) 630-nm thick and b) 940-nm thick.

when the investigated temperature range is considered, the behavior of conductivity may be related to the native defects such as oxygen vacancy in SnO_2. As a result in the above discussion, we have to utilize another electrical conduction model related to disorder rather than grain boundary model for the investigated samples.

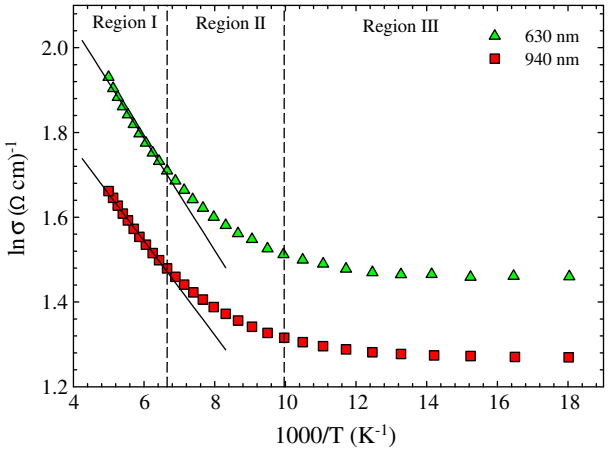

Fig. 4. Temperature dependence of the conductivity plotted as $\ln(\sigma)$ vs. $10^3/T$ in a temperature range 50–200 K. Solid lines are the best-fit lines with Eq. (6).

As can be seen Fig. 4, there is a clear increase in the conductivity values as the temperature increases, a typical characteristic of semiconductor conductivity. However, the increase in the conductivity with temperature is not remarkable. The plots presented in Fig. 4 displayed three distinct regions (regions I–III) presumably corresponding to different conduction mechanisms. Region I typically occupied a temperature region from ~150 K to 200 K where the conductivity increased with the increase in temperature. In this region, we fit the conductivity data to the Arrhenius plot. This may suggest that a simple thermal activation process dominates the electrical conduction in the films. For the thermally activated band conduction, the conductivity (σ) can be expressed as

$$\sigma = \sigma_0 \, exp(-E_a / k_B T) \tag{4}$$

where σ_0 is a constant, E_a is the activation energy and k_B is the Boltzmann's constant.

The values of activation energy obtained from Eq. (4) are very low, which are insufficient for the band conduction from a donor level to conduction band over the temperature range employed. In polycrystalline oxides, oxygen vacancies are known to be the most common defects [17]. The low value of the activation energy shows that the compensation in the samples is appreciably high to exhibit insulating characteristic. In this case, one can expect that the nearest-neighbour hopping (NNH) conduction is dominant in this temperature region. For n-type semiconductors, most of the free electrons are recaptured by the donors at low temperatures. Then the electrons have no sufficient energy to jump from donor levels to conduction band [18,19]. In this case, the band conduction becomes less important, and electron hopping directly between donor states in the impurity band will bring the main contribution to the conduction mechanism [18,19]. When these impurity centers are compensated, hopping conduction becomes possible. Since SnO_2 has the high band gap energy and small Bohr radius, it is possible to observe hopping conduction at even about the room temperature [1,20].

The conductivity of the samples is also lower than Mott's minimum metallic conductivity (σ_{min}) that is given as [2],

$$\sigma_{min} = C\left(\frac{e^2 n_c^{1/3}}{\hbar}\right) \tag{5}$$

where e is the electron charge, $\hbar$ is the Planck constant and n_c is the critical carrier concentration corresponding to the metal-insulator transition. $n_c = 9.54 \times 10^{17}$ cm^{-3} for SnO_2 [1]. C is a numerical constant of the order of 0.03 [2]. The value of $\sigma_{min} = 7.18\ \Omega^{-1}$ cm^{-1} for SnO_2 [1]. Here, we expect that the samples exhibit insulating characteristics with the values of low conductivity ($\sigma < \sigma_{min}$). This allows that the identification of the conduction mechanism related to hopping conduction in the investigated samples. If the compensation is very high, the Fermi level will locate in the impurity band. The conduction of a compensated sample in this case is realized through hopping of charge carriers with very small activation energy directly over impurity states. The conductivity (σ_{NNH}) in the NNH model is given by [21]

$$\sigma_{NNH} = \sigma_1 exp\left(-\gamma / a N_D^{1/3}\right) exp(-E_1 / k_B T) \tag{6}$$

where σ_1 and γ are constants, a is the Bohr radius of the donor wave function, N_D is the donor concentration, and E_1 is the activation energy for electron hopping. From simple potential considerations E_1 would be estimated using the following equation [21]

$$E_1 = \frac{0.99 e^2 N_D^{1/3}}{4\pi\varepsilon} \tag{7}$$

where ε ($\varepsilon = 11.65$ for SnO_2) is the low frequency dielectric constant. The values of E_1 corresponding to E_a are extracted from the slopes of the curves in Fig. 4 and given in Table 2. Utilizing the values of E_1 obtained from Eq. (6), the theoretical values of N_D are obtained by Eq. (7).

The deviations from the straight line in the NNH plot shows that the NNH conduction is not dominating in the lower temperature range. Regions II and III were characterized by the variable-range hopping (VRH) models. According to Mott, electron hopping between nearest neighbor sites is not always favored at low temperatures as the levels may be significantly different in energy. It is possible that electrons can prefer to move to a more energetically similar remote site. In this regime, the following conduction law is expected for the variation of the conductivity (σ_{VRH}) of disordered systems [2,3]:

$$\sigma_{VRH} = \sigma_2 exp(-T_0/T)^s. \quad (8)$$

Here, σ_2 is the pre-exponential factor and, T_0 is a characteristic temperature. The value of the exponent s depends critically on the nature of hopping process. In practice, on hopping conduction it is assumed that σ_2 in Eq. (8) is independent of the temperature. However, hopping theory predicts that $\sigma_2(T) = \sigma_2 T^{-2s}$ [22,23]. When the VRH mechanism dominates the conduction, the condition $0 < s < 1$ is fulfilled. If the density of states around the Fermi level assumed to be constant, s becomes $s = 1/4$ (Mott VRH). On the other hand, if there is a gap at the Fermi level, the VRH conduction model is expressed with $s = 1/2$ in Eq. (8) (Efros–Shklovskii (ES) VRH) [2,3].

Fig. 5 shows the plot of $\ln(\sigma T^{1/2})$ against $T^{-1/4}$. The plot of $\ln(\sigma T^{1/2})$ vs. $T^{-1/4}$ was found to have been linear at temperatures (100–150 K). This indicates that the conduction in SnO_2 thin films is governed by Mott's VRH ($T^{-1/4}$ law) conductivity instead of the NNH at high temperatures. As the temperature decreases below nearly 100 K, there is a deviation from a conduction mechanism to another one. At lower temperatures ($T < 100$ K), when the measured data were plotted as $\ln(\sigma T)$ vs. $T^{-1/2}$ (inset of Fig. 5) as indicated by the ES VRH $T^{-1/2}$ law, well defined lines were obtained. Therefore, regions II and III were characterized by Mott VRH and ES VRH models, respectively.

It is caused by hopping conduction between defects of localized states in the grain boundary space-charge region. The existence of the localized states for such a conduction process is a consequence of imperfections associated with polycrystalline films. In polycrystalline materials, the VRH conduction process exists in the grain boundaries at temperatures at which the carriers do not have sufficient energy to cross the potential barrier and to transfer themselves into the crystallite by the process of thermionic emission [24,25].

Region II is characterized by Mott's relation [2],

$$\sigma_{VRH,Mott} = \sigma_{2,Mott} T^{-1/2} \, exp\left(-T_{0,Mott}/T\right)^{1/4} \quad (9)$$

where

$$\sigma_{2,Mott} = \frac{3e^2\nu}{(8\pi)^{1/2}} \left[\frac{\xi N(E_F)}{k_B}\right]^{1/2}. \quad (10)$$

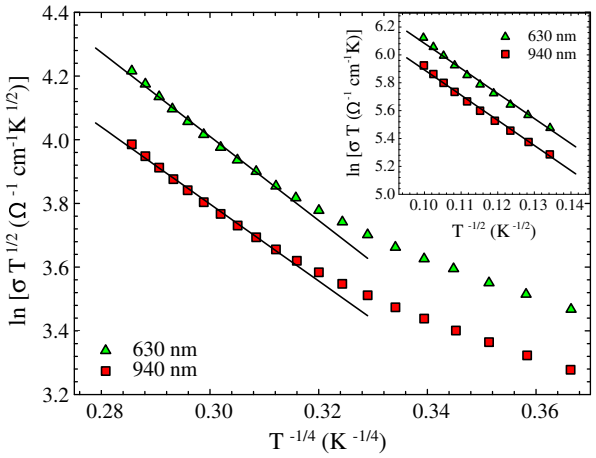

Fig. 5. Temperature dependence of the conductivity plotted as $\ln(\sigma T^{1/2})$ vs. $T^{-1/4}$. Solid lines are the best-fit lines with Eq. (9). The inset of Fig. 2 represents the conductivity plotted as $\ln(\sigma T)$ vs. $T^{-1/2}$. Solid lines are the best-fit lines with Eq. (13).

$T_{0,Mott}$ is a characteristic temperature coefficient which depends on the density of states $N(E_F)$ at the Fermi level in the form [2]:

$$T_{0,Mott} = \frac{18}{k_B \xi^3 N(E_F)}, \quad (11)$$

where ξ is the localization length and ν is the typical phonon frequency. The values of $T_{0,Mott}$, and $\sigma_{2,Mott}$ obtained from the slope of the curves of Fig. 5, are given in Table 3. Using these values, $N(E_F)$ and ξ are obtained from Eqs. (10) and (11), and given in Table 3. Here ξ is of the order of 1 nm, which is consistent with the expected magnitude in the VRH regime [26]. The values of $N(E_F)$ also matched with that reported for SnO_2 which confirms that Mott VRH hopping dominates in the employed temperature region [27]. As the film thickness is increased the crystallite size increases in our films. In such a case, the conductivity behavior in polycrystalline materials can be inferred by grain boundary model [25]. However, there is an increase of the conductivity, with the decrease in the thickness of the films from 940 to 630 nm. Therefore, grain boundary model is not valid for the investigated films as previously mentioned. We consider the VRH conduction to explain the effect of film thickness to conductivity. The initial value of $N(E_F)$ increases with decreasing thickness. This leads to an improvement in conductivity by less than a factor of 2, which corresponds to only a slight modification in the $N(E_F)$. Since the $N(E_F)$ increases and becomes more localized, it should be expected as an increase in the conductivity with decreasing film thickness.

As mentioned previously, the impurity band conduction appeared in disordered or highly compensated materials. In order to corroborate the estimated models for understanding the electrical conduction, we can determine the critical temperatures (T_{c1}) for transition from the NNH to the Mott VRH by knowing the values of ξ. T_{c1} has been calculated by Shklovskii [11]. According to Shklovskii, this

Table 2
The experimental NNH activation energy (E_1), the critical temperature (T_{c1}) for transition from the NNH to the Mott VRH, donor concentration (N_D), acceptor concentration (N_A), compensation ratio (k) for the investigated SnO_2 films.

Sample	E_1 (meV)	T_{c1} (K)	N_D (cm^{-3})	N_A (cm^{-3})	k
Thickness (630 nm)	11.02	144	7.09×10^{17}	4.3×10^{17}	0.606
Thickness (940 nm)	9.42	143	4.43×10^{17}	3.3×10^{17}	0.745

Table 3
Values of the Mott VRH conduction parameters and the critical temperature (T_{c2}) for transition from the Mott VRH to the ES VRH.

Sample	$T_{0,Mott}$ (K)	$\sigma_{2,Mott}$ (Ω^{-1} cm^{-1})	ξ (nm)	$N(E_F)$ (cm^{-3} eV^{-1})	T_{c2} (K)	$R_{hop,Mott}$ (nm)
Thickness (630 nm)	2.81×10^4	2.25×10^3	1.26	3.71×10^{21}	105	1.63
Thickness (940 nm)	2.69×10^4	1.67×10^3	1.72	1.52×10^{21}	101	2.21

Table 4
Values of the ES VRH conduction parameters.

Sample	$T_{0,ES}$ (K)	$\sigma_{2,\ ES}$ (Ω^{-1} cm^{-1})	ξ (nm)	$R_{hop,ES}$ (nm)
Thickness (630 nm)	429	3.57×10^{3}	9.35	2.83
Thickness (940 nm)	411	2.81×10^{3}	9.76	2.92

equation is applicable when compensation ratio becomes high (k>0.5).

$$T_{c1} = e^2 N_D^{2/3} \xi / k_B(4\pi\varepsilon\varepsilon_0). \quad (12)$$

Taking the values of N_D and ξ, the values of the T_{c1} are determined. These values are collected in Table 2. These values are not so far from the temperatures where the transition from the NNH to the Mott VRH conduction is experimentally observed for the investigated samples. It is obvious that the theoretical finding is consistent with the experimental observations.

Region III is characterized by the ES VRH model [3],

$$\sigma_{VRH,ES} = \sigma_{2,ES} T^{-1} exp\left(-T_{0,ES}/T\right)^{1/2}. \quad (13)$$

$T_{0,ES}$ is a characteristic temperature coefficient given by [3],

$$T_{0,ES} = \frac{2.8e^2}{k_B \xi \varepsilon}. \quad (14)$$

In order to determine the values of $\sigma_{2,ES}$ and $T_{0,ES}$, the conductivity data were fitted by Eq. (13). By this way, $\sigma_{2,ES}$ and $T_{0,ES}$ have been obtained. The results of fitting are given in Table 4. The values of the localization length (ξ) in the ES VRH regime are higher than as in the Mott VRH regime. The values of $T_{0,Mott}/T$ and $T_{0,ES}/T$ are found to be greater than one for both samples, confirming the validity of the Mott and the ES VRH conductions in the investigation of temperature regions [2,3].

The critical temperatures (T_{c2}) for transition from the Mott VRH to the ES VRH can be also calculated by knowing the values of $T_{0,ES}$. This transition is expected when the average hopping energy (Δ_{hop}) has the same value for two regimes. The values of the average hopping energy (Δ_{hop}) are calculated from Eqs. (15) and (16) in the Mott VRH and the ES VRH regimes, respectively [2,3].

$$\Delta_{hop,Mott} = \frac{1}{4} k_B T \left(T_{0,Mott}/T\right)^{1/4} \quad (15)$$

$$\Delta_{hop,ES} = \frac{1}{2} k_B T \left(T_{0,ES}/T\right)^{1/2}. \quad (16)$$

Setting Eqs. (15) and (16) equal to each other, this yields

$$T_{c2} = 16 T_{0,ES}^2 / T_{o,Mott}. \quad (17)$$

We calculated the values of T_{c2} from Eq. (17) for the investigated samples. Well agreements between the estimated transition temperature T_{c2} from Eq. (17) and the experimental values were found (Table 3). Actually, the deviation from the Mott VRH is also experimentally observed about 100 K for both samples.

The film thickness (d) is a significant parameter in order to decide whether the dimensionality of VRH is three dimensional (3D) or not. The hopping distance (R_{hop}) is also a characteristic parameter for the VRH conduction. It was described in Refs. [2,3,23]. The calculated values of R_{hop} were given in Tables 3 and 4. Since our films are of 3D, the condition ($d >> R_{hop}$) is fulfilled at both Mott and ES regime for the films [2,3].

The hopping conduction can be fulfilled only by donor–acceptor compensation. The knowledge of $N(E_F)$ allows us to calculate the compensation ratio which characterizes the degree of disordered. High compensation is responsible for observation of the impurity band conduction. Finally, we can obtain the compensation ratio (k) and then acceptors concentration (N_A) using an expression valid for a compensated material in case of k>0.5 [20];

$$N(E_F) = \left(2\varepsilon / e^2\right) N_D^{2/3} (1-k)^{4/3}. \quad (18)$$

Substituting the values of $N(E_F)$ and N_D into Eq. (18), the values of the k and then N_A are also determined. Their values are collected in Table 4. The decrease in compensation ratio reflects the value of conductivity. Since the value of k is the degree of disorder in the material, the decrease in the value of k results in a decrease in disorder of the films [2,3]. Then, this leads to an increase in conductivity of SnO_2 thin films.

4. Conclusion

This study demonstrates that the conductivity in SnO_2 thin films at low temperatures (50–200 K) can be seen to follow different hopping conduction mechanisms for different temperatures regions. We have used a theoretical approach, based on the hopping conduction models, that makes it possible to identify the presence of different hopping conduction mechanisms as the main reason in electrical conduction through SnO_2 thin films. It is important to note that the experimentally determined critical transition temperatures are orders of magnitudes with what could be expected based on hopping conduction calculations. After these analyses, various electrical parameters of the present samples such as donor concentration, density of states at the Fermi level, acceptor concentration and then compensation ratio were determined. It was found that a decrease in the compensation ratio results in an increase in conductivity of SnO_2 thin films.

Acknowledgements

This work is supported by the State of Planning Organization of Turkey under Grant No. 2001K120590 and the Ankara University BAP under Project Number 2007-07-45-054. We would also like to thank Prof. Dr. Yusuf Kağan Kadıoğlu and Ms. Murat Yavuz for providing XRD and AFM measurements.

References

[1] T. Serin, A. Yildiz, N. Serin, N. Yıldırım, F. Özyurt, M. Kasap, J. Electron. Mater. 39 (2010) 1152.
[2] N.F. Mott, E.A. Davis, Electronic Properties in Non-crystalline Materials, Clarendon Press, Oxford, 1971.
[3] A.L. Efros, B.I. Shklovskii, Electronic Properties of Doped Semiconductors, Springer, Berlin, 1984.
[4] A. Yildiz, N. Serin, T. Serin, M. Kasap, Jpn. J. Appl. Phys. 48 (2009) 111203.
[5] A. Yildiz, S.B. Lisesivdin, M. Kasap, D. Mardare, Phys. B 404 (2009) 1423.
[6] A. Yildiz, S.B. Lisesivdin, M. Kasap, S. Ozcelik, E. Ozbay, N. Balkan, Appl. Phys. A 98 (2010) 557.
[7] R. Swanepoel, J. Phys. E Sci. Instrum. 16 (1983) 1214.
[8] Powder Diffraction File. International Center for Diffraction Data, Newtown Square, PA (formerly Joint Committee on Powder Diffraction Standards, Swarthmore, PA, 1991): No. 41–1445.
[9] B.D. Cullity, Elements of X-ray Diffraction, 2nd ed.Addison-Wesley, Reading, MA, 1978.
[10] D. Fröhlich, R. Kenklies, R. Helbig, Phys. Rev. Lett. 41 (1978) 1750.
[11] J.C. Tauc, A. Menth, J. Non-Cryst. Solids 569 (1972) 8.
[12] P. Rajaram, Y.C. Goswami, S. Rajagopalan, V.K. Gupta, Mater. Lett. 54 (2002) 158.
[13] C. Terrier, J.P. Chatelon, J.A. Roger, Thin Solid Films 295 (1997) 95.
[14] T. Serin, N. Serin, S. Karadeniz, H. Sarı, N. Tugluoglu, O. Pakma, J. Non-Cryst. Solids 352 (2006) 209.
[15] J.Y.W. Seto, J. Appl. Phys. 46 (1975) 5247.
[16] J.W. Orton, M.J. Powel, Rep. Prog. Phys. 43 (1980) 1263.
[17] J. Ma, Y. Wang, F. Ji, X. Yu, H. Ma, Mater. Lett. 59 (2005) 2142.
[18] A. Miller, E. Abrahamas, Phys. Rev. 120 (1960) 745.
[19] R.A. Street, Hydrogenated Amorphous Silicon, Cambridge University Press, Cambridge, 1991.

[20] A.J.C. Lanfredi, R.R. Geraldes, O.M. Berengue, E.R. Leite, A.J. Chiquito, J. Appl. Phys. 105 (2009) 023708.
[21] B.I. Shklovskii, Sov. Phys. Semicond. 6 (1973) 1053.
[22] R. Mansfield, Philos. Mag. B 57 (1988) 777.
[23] A. Yildiz, S.B. Lisesivdin, M. Kasap, D. Mardare, J. Non-Cryst. Solids 354 (2008) 4944.
[24] M.M. Abdul-gader, M.A. Al-basha, K.A. Wishah, Int. J. Electron. 85 (1998) 21.
[25] A. Yildiz, N. Serin, M. Kasap, T. Serin, D. Mardare, J. Alloy. Comp. 493 (2010) 227.
[26] H. Fritzsche, in: J. Tauc (Ed.), Amorphous and Liquid Semiconductors, Plenum, London, 1974.
[27] K. Dutta, S.K. De, J. Phys. D Appl. Phys. 40 (2007) 734.